Asymmetric variable stiffness powered ankle (AVSPA) prosthesis for advanced musculoskeletal interfacing

Haoran Sun, Chaoming He, Ivan Vujaklija, *Member, IEEE*

Abstract*— *Objective: **We propose a low-profile powered asymmetric variable stiffness ankle prosthesis with both binary and continuous stiffness adjustment.** ***Methods:*** **Independent torque/position and stiffness control is achieved using two actuators. Inspired by ankle biomechanics, the joint is designed to have two stiffness adjustment modes: active continuous regulation and passive binary change as gait phases are switching. The former is realized via the adjustable effective length of leaf springs through changing the contact points between rollers and springs themselves. The latter is implemented using springs with asymmetric stiffness in different directions of ankle flexion. The self-locking property of the lead screw is used to retain the roller position, thus maintaining the desired stiffness in an energy efficient manner.** ***Results:*** **System identification experiments demonstrate that the proposed prototype behaves in a desirable way for a prosthesis throughout stiffness and torque adjustment scenarios across operating modes (passive, semi-active, active). Additionally, the potential for clinical translation has been demonstrated through a mockup interfacing scenario within which the real-world walking data has been used to emulate effective prosthesis control in a simulated walking scenario.** ***Conclusion:*** **The proposed asymmetric variable stiffness powered ankle prosthesis with binary stiffness switching and continuous stiffness adjustment has a potential of delivering close to natural biomechanical behavior, while retaining low profile and energy efficient operation.** ***Significance:*** **To our knowledge, this is the first powered ankle prosthesis with asymmetric variable stiffness design which considers ankle biomechanics between and during specific gait phases, thus opening up new avenues for applying compliant powered ankle prostheses.**

***Index Terms*—prosthetic ankle, variable stiffness, amputee gait, powered prosthesis, series elasticity.**

I. Introduction

Globally, there are an estimated 35.3 million people living with lower limb amputations caused by traumas [1], and many more resulting from diabetic foot sepsis, peripheral vascular disease, and neoplasms [2]. As predicted by World Health Organization (WHO), the number of amputees is likely to double by 2030 with an aging global population and a rise in noncommunicable diseases [3]. Therefore, there is a rapidly growing demand for artificial limbs able to sufficiently support and ease societal reintegration of those in such need.

Limb substitution through passive prostheses is a common and robust approach to aid those with lower limb impairments. However, these non-actuated devices can only partially meet the demands of assisted locomotion. The absence of additional mechanical power limits the range of activities that can be supported, resulting in the reduced quality of life with often negative physical, psychological, and social implications for amputees [4]. Hence, it comes as no surprise that over the past few decades, both academics and industry were eager to design and offer powered lower limb prosthesis able to restore the natural biomechanics and provide functional versatility [4]–[8]. While these solutions target different levels of lower limb disabilities, the design (powered or otherwise) of ankle joint plays an indispensable role across the majority of them. This is due to the naturally varying compliance of the intact ankle in response to distinct walking conditions and the ankle's pivotal role in propelling the body forward throughout the gait cycle [9], [10].

When featuring a properly tuned mechatronic system, powered ankles have a potential to both support suitable limb behaviors during gait, as well as reduce human energy consumption [11]. For passive ankle prosthesis, elastic foot designs have been rather appreciated due to the energy storage-and-return ability [12]. By applying elastic elements, it is possible to store negative mechanical work in prosthetic ankles and release it as mechanical energy while facilitating more compliant movements [11]–[16]. Naturally, elastic feet, such as carbon fiber foot, are adopted also by some powered ankles [13], [14] in order to provide series-elasticity to the robotic ankle-foot complex. Moreover, the featured elasticity allows these ankles to compensate for the deficiency of direct-driven joints in terms of compliance and energy storage capacity. Alternatively, a direct integration of series-elasticity into the

This work was supported by the Sichuan Science and Technology Program under Grant 2021YFS0065. *Asterisk indicates corresponding author.*

H. Sun is now with the School of Mechanical Engineering, Southwest Jiaotong University, Chengdu 610031, China. He was with the Department of Electrical Engineering and Automation, Aalto University, Espoo 02150, Finland. (e-mail: sunhaoran@my.swjtu.edu.cn)

C. He is with the School of Mechanical Engineering, Southwest Jiaotong University, Chengdu 610031, China. (e-mail: hcm@swjtu.edu.cn)

*I. Vujaklija is with the Department of Electrical Engineering and Automation, Aalto University, Espoo 02150, Finland (e-mail: ivan.vujaklija@aalto.fi).

ankle actuator itself can be done. For instance, Hollander et al. [15] and Hitt et al. [16] employ a series-elastic actuator (SEA) consisting of a helical spring in series with a motor, which stores mechanical negative work during controlled dorsiflexion (CD) in the spring and then releases it during the powered plantar flexion (PP). This effectively decreases the required peak power for the motor. The series-elasticity approach endows the ankle with energy storage capacity and achieves better performance in terms of energy and compliance, which has become a significant point of interest.

However, it should be noted that the stiffness of a leg is adjusted whenever the activity or the contact surface changes [11], [17], [18]. In fact, the ratios between ankle torque and ankle-foot angle change across gait phases in order to assist different objectives during level-ground walking [17], [19], [20] – absorbing the impact, storing and releasing the energy, etc.. The modulation of the torque-angle relationship of the human ankle joint, which is nonlinear in nature, is not likely to be effectively simulated using aforementioned serial elastic elements with constant stiffness [13]–[16]. This has led to the design of multiple stiffness adjustment structures in hope of achieving an improved active prosthesis experience. Au et al. [11], [21] proposed a powered ankle-foot which combines, in parallel, a SEA with a configured unidirectional spring. While transitioning from heel-strike to mid-stance, only the spring of SEA acts to suppress the impact, while after equilibrium position, the parallel spring works as well to provide additional stiffness and store more energy. Hence, the design passively achieves a variable joint stiffness by switching between one and two springs as the gait changes. However, biomechanical studies have shown that ankle joint stiffness varies with not only gait phases but also walking speeds [10], [22], movement patterns [22], changing terrains [23], [24], and surface stiffness [25], [26]. For example, ankle joint stiffness increases during running compared to walking and demonstrates a positive correlation with running speed [22]. To account for this behavior, the variable stiffness actuator (VSA) is introduced into the lower-limb prosthesis. For instance, CYBERLEG's Alpha [27]–[29] incorporates a passive knee and an active ankle with variable stiffness characteristics. It changes joint stiffness by changing the pre-extension of the serially integrated spring. However, during adjustment, the regulating mechanism needs to produce high power to offset the reaction force of spring deflection. Hence, the stiffness regulating motor of CYBERLEG's Alpha has a gearbox with a high transmission ratio to generate large power, though in turn it provides lower regulating speed and a degree of energy efficiency.

Presently, actuated ankle prosthetic systems, including those incorporating variable stiffness designs, confront a trade-off involving size, energy efficiency, and functionality. Consequently, amputee prosthetic users often encounter the need to make compromises in their daily experiences.

To address these issues, we propose a compact, energy efficient, gearbox-free asymmetric variable stiffness prosthetic ankle (AVSPA) design which features a variable stiffness actuator (VSA) with both binary stiffness switching and continuous stiffness adjustment. Leaf springs are leveraged to provide variable series elasticity to the joint in this design, achieving stiffness adjustment through either altering the effective length or switching the intrinsic stiffness of the leaf springs. In addition, the self-locking property of the stiffness adjustment screw mechanism makes it possible to maintain the stiffness without power output from motor, which should reduce energy consumption. The benefits of this design have been evaluated both in conventional table-top tests as well as by applying real-world estimates derived from musculoskeletal observations.

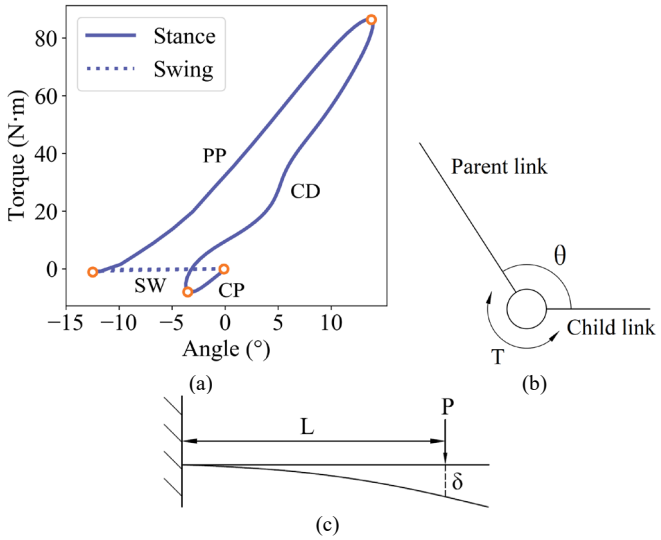

Fig. 1. (a) Average ankle torque is plotted versus angle, using the data of N=6 individuals walking at a speed between 0.8 and 1.2 m/s, from a dataset established on injury-free adult participants [20]. CP: Controlled plantar flexion; CD: Controlled dorsiflexion; PP: Powered plantar flexion; SW: Swing phase. (b) Schematic diagram of a robotic joint (c) A leaf spring fixed at one end is deformed by force P at an effective length L with a deflection of δ, which is modelled equivalent to a cantilever beam.

II. AVSPA Modelling and Mechanical Design

A. Modeling

In order to design a prosthetic structure that conforms to biological ankle behavior, we established a model for the core structure (stiffness adjustment mechanism) of AVSPA after analyzing biomechanical data of intact ankle joints. From the biomechanical data [20] plotted in Fig. 1, we observed that the ankle joint behavior during controlled plantar flexion (CP) phase is consistent with a linear torsional spring whose torque proportional to angle. However, ankle joint behavior during CD and PP periods can be approximated as nonlinear springs. In addition, when the switching occurs between CP and CD phases, the quasi-stiffness changes rapidly with the direction of rotation.

For the purposes of ankle prosthesis design, the equivalent stiffness K can be represented as Equation 1:

$$K = \frac{T}{\Delta\theta} \tag{1}$$

where $\Delta\theta$ is the angular deformation between parent and child links of the joint caused by the torque T (Fig. 1b).

Therefore, the equivalent stiffness K can be changed by varying the angular deformation $\Delta\theta$ under a certain load. For robotic joints, this angular deformation $\Delta\theta$ can be achieved by

employing elastic elements inside the joints that generate circumferential deformation around the center of joint rotation.

Leaf springs are a type of elastic element typically made of resilient materials in the form of plates, sheets, or strips. By employing leaf springs as elastic components of robotic joints, adjustable deflection can be realized and then be transformed into adjustable angular deformation of the joint, in a simple and efficient way [30]–[32]. By moving the position of the loading point along the leaf spring, the deflection perpendicular to the direction of the leaf spring can be adjusted (Fig. 1c). The deflection δ of the leaf spring at the loading point can be expressed as the formula for a cantilever beam under a concentrated load, which is shown as Equation 2:

$$\delta = \frac{PL^3}{3EI} \tag{2}$$

where P is the magnitude of the concentrated load, L is the distance between the loading point and the fixed point (the effective length of the spring), E is the Young's modulus determined by the material of the leaf spring, while I is the area moment of inertia determined by the shape and dimension of the cross section of the leaf spring.

It can be inferred from Equation 2 that, when the load remains constant, the deflection is related to the product of the Young's modulus E and the area moment of inertia I, as well as the effective length L of the spring. With this in mind, and upon revisiting the gait cycle analysis of intact ankle biomechanics, we proposed the concept model for the asymmetric variable stiffness mechanism (Fig. 2a).

Firstly, by arranging the axis of the leaf springs towards the center of the joint rotation, the joint torque is converted into a concentrated load applied perpendicularly to the leaf spring through the rollers H. Correspondingly, the angular deformation caused by the joint torque comes out of the deflection of leaf springs.

Subsequently, the stiffness response of the ankle prosthesis can be harmoniously aligned with ankle biomechanics through the following means. In CD and PP phases of the gait cycle, the continuous adjustment of angular deformation and stiffness can be achieved by regulating the position of the roller along the leaf spring. This results in the continuous change of the effective length x (Fig. 2a) and the deflection of the leaf spring, in order to simulate the nonlinear spring behavior of the intact ankle in CD and PP phases. Moreover, during the transition from the CP to CD phase, a substantial increase occurs in the quasi-stiffness of the intact ankle joint, together with a change in the direction of ankle flexion. Therefore, in our model, we employ a "spring-roller-spring" (SRS) configuration (Fig. 2a), which enables the asymmetric variable stiffness to be achieved by arranging leaf springs with different Young's modulus and/or moment of inertia ($E \cdot I$) on either side of the roller. With the asymmetric design, the roller contacts with leaf springs of different intrinsic stiffness depending on the direction in which the spring rotates around joint center O (i.e., plantar- and dorsi- flexion directions), resulting in binary stiffness switching during the transition between CP and CD in a simple and rapid manner.

In order to obtain the theoretical equivalent stiffness of the

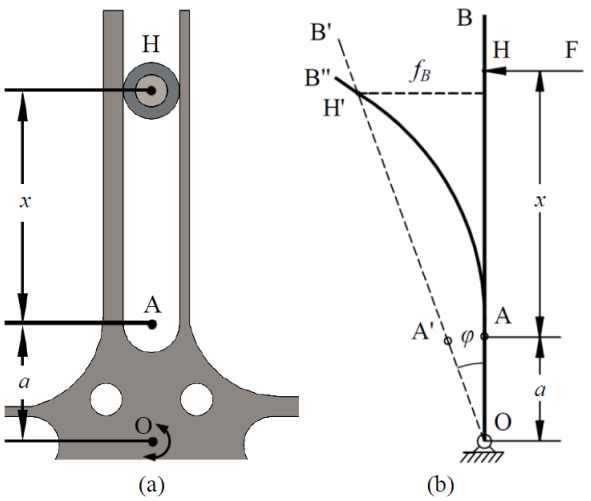

Fig. 2. Models of the asymmetric variable stiffness mechanism. (a) Diagram of roller-spring contacting. The "spring-roller-spring" (SRS) arrangement enables the use of asymmetric stiffness springs. (b) Cantilever beam model of leaf spring. The principle of stiffness modulation: when the roller is repositioned, the effective length x of the leaf spring varies, which leads to a different angular deformation φ of the joint.

system, the contact model is simplified into the cantilever beam diagram as shown in Fig. 2b. The OA section can be regarded as a rigid part, and the AB section is the leaf spring. When the roller locates at point H, AB is deformed into AB″ by the force F perpendicular to the beam at point H. When the spring rotates around point O by the angle φ, the spring OAB undergoes deformation into shape OAB" due to the restriction of the roller, and the deflection at point H is denoted as f_B. The distance between roller and the plane center O of VSA remains unchanged, that is, $\mathrm{OH} = \mathrm{OH}' = x + a$.

Taking into consideration the concept of the equivalent cantilever in Equation 2, the theoretical equivalent stiffness K of the system using the design depicted in Fig. 2, can be represented as Equation 3.

$$K \doteq \frac{3nEI(x+a)^2}{x^3} \tag{3}$$

where x represents the effective length of the leaf spring, a the distance from the fixed point of the leaf spring to the center of rotation, and n the number of pairs of asymmetric leaf springs placed around the joint center.

Subsequently, this stiffness adjustment concept is implemented into a mechanical design of AVSPA, while the mathematical stiffness model (Equation 3) provides a theoretical foundation for the controller design in the initial use case demonstrations and evaluations.

B. Mechanical Design

The implemented structure of the proposed AVSPA is shown in Fig. 3. Four pairs of asymmetric leaf springs are evenly distributed around the center of rotation, forming the cross spring (7). Therefore, the parameter n in Equation 3 equals to 4 in this context. Leadscrew mechanisms (3) are adopted to synchronously move roller components (5) and effectively change the contact points between rollers and the cross spring (7), resulting the adjustable equivalent stiffness. Specifically, after the stiffness adjustment command is issued, the secondary

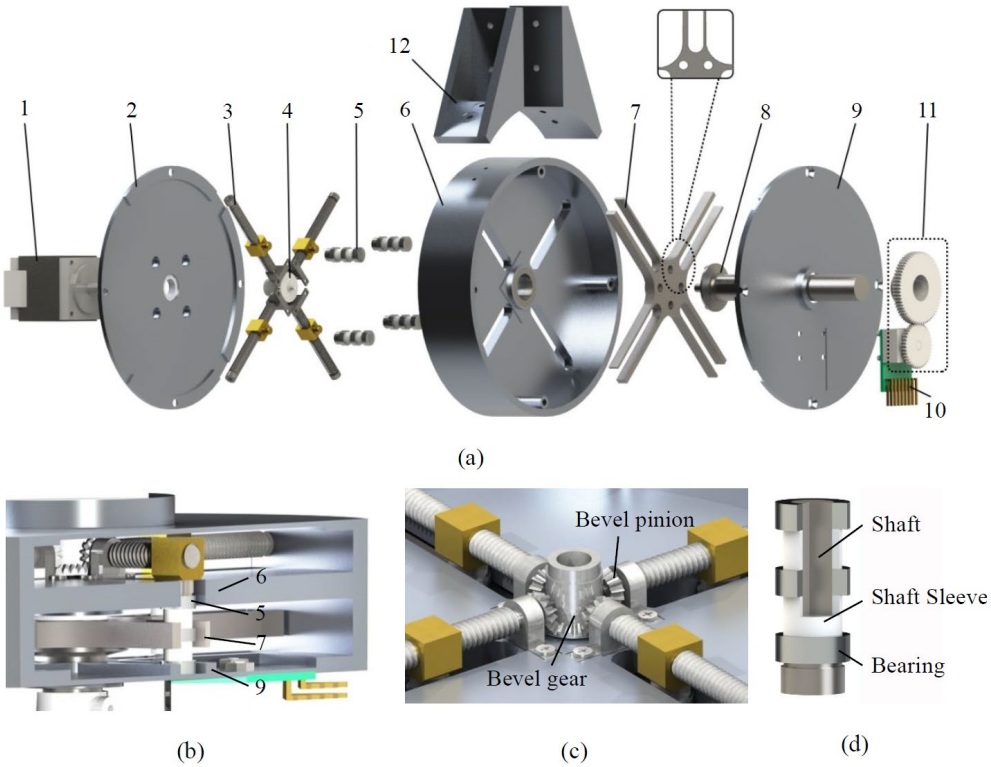

Fig. 3. The structure of our prototype: (a) Exploded view; (b) Roller components which are rigidly attached on the sliders, move along straight grooves as leadscrews are actuated. Inside the VSA, load is transmitted from spring via roller components to the walls of straight grooves which is part of the output frame. (c) Each leadscrew is rigidly connected to a bevel pinion, and driven by a bevel gear. (d) Roller components (including bearings, a shaft, and shaft sleeves for locating bearings).

motor (1) is controlled to drive bevel gear (4), and then leadscrew mechanisms (3) are synchronously driven through the bevel pinions (shown in Fig. 3c). Roller components (5) are rigidly attached on the sliders of leadscrew mechanisms (3), and placed in the straight grooves of the output frame (6) and the straight gaps between leaves of cross spring (7), so that the effective length of the spring changes when the leadscrew mechanisms (3) are actuated. The angular deformation between input shaft (8) and output frame (6) is measured by magnetic rotary encoder (10) through the gear pair (11) one of which is rigidly installed on the input shaft (8). In the implementation, a principal motor is connected to input shaft (8), and an artificial foot is fixed within a gripper (12) which is installed on output frame (6).

The effective stiffness switching also relies on the self-locking feature of the lead screw mechanism. As a result, the rollers can remain still even though the secondary motor is turned off when the load increases. This property enables AVSPA to maintain stiffness in all operation modes without activating the secondary motor, thus reducing energy consumption.

Fig. 3b shows the inner assembly of the regulating mechanism, demonstrating the contact relationship among the inner components. As can be seen, roller components are made of a rigid shaft with several bearings and shaft sleeves mounted on. Torque is transmitted from input shaft (8) which is rigidly connected with cross spring (7), and then to roller components (5) which actuate output frame (6).

III. Materials and Methods

A. Practical Implementation

The cross spring which consists of four pairs of asymmetric leaf springs is shown in Fig. 4b. The corresponding leaf springs are made out of 55-Nitinol martensite with different thicknesses on either side of the roller. This results in the springs with the same Young's module $E = 50$ GPa and two different area moments of inertia $I = 0.094$ mm^4 and 0.188 mm^4 on the working sides of the CP and CD phases respectively.

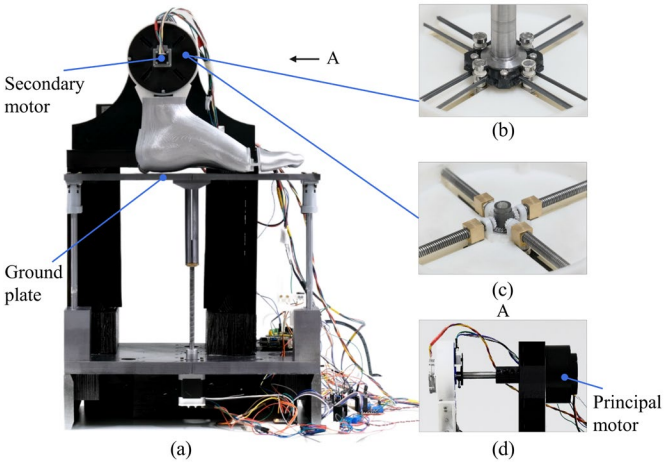

Fig. 4. The manufactured prototype of the AVSPA with a 3D printed foot attached. (a) Overview of the test bench (b) SRS arrangement implemented physically (c) Lead screw mechanism corresponding to Fig. 3c (d) A-direction partial view

We utilized a dynamic module AK80-80 (T-motor, China) as the principal motor in our system (Fig. 4d). This module integrates a brushless DC (BLDC) motor, an electronic speed controller (ESC) based on the three-phase integrated BLDC motor driver DRV8323 (Texas Instruments, USA), a rotary encoder AS5047P (ams-OSRAM AG, Austria) with a resolution of 4000 counts per revolution (cpr), and a set of planetary gears with a transmission ratio of 80:1. The module was powered by a 24V source. In addition, a stepper motor PKP225D15A2-R2EL (Oriental motor Ltd., Japan), which has a built-in rotary encoder (200 cpr), was used as the secondary motor for stiffness regulating (Fig. 4a). Besides, an additional rotary encoder AS5047P is installed on the output frame to measure the angular deformation between the input shaft and the output frame caused by the series-elasticity from leaf springs.

The control of the described electromechanical system is deployed on a dedicated microcontroller system. As shown in Fig. 5, the Raspberry Pi 4B (Raspberry Pi Ltd., UK) receives kinematic and/or kinetic data stream from human machine interface (HMI), then generates desired trajectories of joint position and stiffness, and transmits motor position control commands P_p^{des} and P_s^{des} to controllers. It also receives feedback of P_p^{real}, P_s^{real} and $\Delta\theta$, which indicate the real positions of principal and secondary motors, and the angular deformation, from multiple encoders.

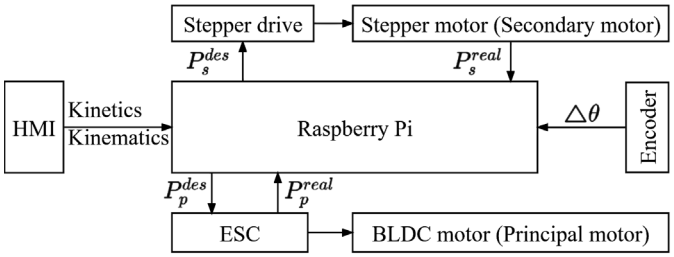

Fig. 5. Overview of the embedded hardware configuration. Raspberry Pi is connected to multiple hardware, and serves as a central hardware controller, which achieves the functions of data collection, calculation, and recording, as well as control commands generation and transmission.

B. Controller design

As the fundament of the controller design for the actuation system, it is helpful to understand the influence of controllable factors on the prosthesis behavior. Herein, Equation 1 is expanded into Equation 4, since the angular deformation $\Delta\theta$ in Equation 1 can be interpreted as the difference between the ankle-foot angle and the equilibrium angle in the prosthetic system.

$$T = K \cdot (\theta_{eq} - \theta) \quad (4)$$

where T denotes the joint torque, K the equivalent stiffness, θ the ankle-foot angle during the operation of AVSPA, and θ_{eq} the equilibrium angle which is the ankle-foot angle when the springs on both sides of the roller inside AVSPA are not bent.

In Equation 4, the equilibrium angle θ_{eq} is controlled by the position of the principal motor P_p^{real} through a transmission ratio, while the stiffness K is adjusted by the lead screw mechanisms driven through the position of the secondary motor

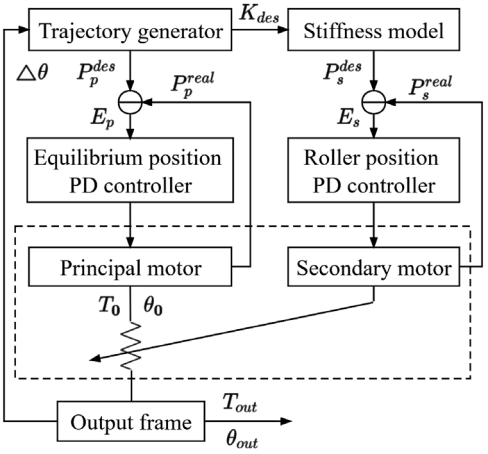

Fig. 6. Controller architecture for AVSPA. Motor control commands P_p^{des} and P_s^{des} are generated through trajectory generator and the stiffness model (top of the diagram). Principal and secondary motor are simultaneously controlled via independent PD controllers. The errors of motor position control E_p and E_s are fed back to corresponding PD controllers, while the angular deformation $\Delta\theta$ is fed back to the trajectory generator, enabling the states of the entire system to be identified in the control framework.

P_s^{real} (Fig. 4). The ankle-foot angle θ can be actively regulated by adjusting the equilibrium angle θ_{eq} when the artificial foot is off the ground. The precision of its positional control is influenced by the equivalent stiffness K. However, when the foot comes into contact with the ground, the ankle-foot angle undergoes a passive metamorphosis, beholden to the constraint imposed by the ground. In *In-vitro gait demonstration and analysis* of *Experimental evaluation*, we provide further details on the change of these controllable factors during the prosthesis operation.

As shown in Fig. 6, after receiving input data flow, a trajectory generator internally solves the trajectory of ankle-foot angle θ, desired torque T, and equivalent stiffness K through inverse kinematics and dynamics. Then the desired positions of principal and secondary motors P_p^{des} and P_s^{des} are estimated from θ, T, and K, using Equations 3 and 4 and transmission ratios. Subsequently, the P_p^{des} and P_s^{des} are sent to PD controllers. For both controllers, the errors between the desired and the real angular positions serve as feedbacks, which are $E_p = P_p^{des} - P_p^{real}$ and $E_s = P_s^{des} - P_s^{real}$.

C. Experimental evaluation

In order to investigate the properties of the proposed prototype and validate that the design can meet the requirements of eventual prosthetic use, a range of system identification and mock use case application experiments have been executed.

1) System identification

System identification was conducted in order to determine the operational limitations of the AVSPA system and to characterize its behavior as to retrieve insights for subsequent controller design.

1.1) Stiffness measurement

Through stiffness measurement experiments, the range and

variability of the system stiffness were observed and characterized. By adjusting the secondary motor, the rollers were gradually moved across 11 evenly spaced positions in the entire roller range, i.e., x = [0, 3.5, 7, 10.5, 14, 17.5, 21, 24.5, 28, 31.5, 35] mm (see Fig. 2). At each roller position, the principal motor was rotated to 10 angular positions in clockwise and counter-clockwise directions from -90° to 90°, to adjust the loading torque covering the range of [-1.67, 1.67] N·m. The roller position x, loading torque T, and angular deformation $\Delta\theta$ were continuously observed in order to estimate the equivalent stiffness K both from the derived theoretical model (Equation 3) and from the directly observable stiffness definition (Equation 1).

1.2) Sinusoidal tracking for position control

Sinusoidal tracking experiments were performed to identify the boundary conditions of the dynamic system operation. Initially, the sinusoidal period sweeping was used in order to determine the maximum speed and acceleration reliably achievable by the principal motor under the experimental configuration. Ten different sinusoidal cycle lengths (0.6s, 0.8s, 1.25s, 2s, 2.5s, 3s, 4s, 5s, 6s, 7s, and 8s), were used covering the [-90°, 90°] range. Throughout the experiments, the maximum stiffness was maintained in order to provide a rigid connection between the load and the motor, and minimize the influence of series elasticity.

When the foot is not in the contact with the ground plate (see Fig. 4), such as during the swing phase of a gait cycle, the system kinematics is dependent not only on the speed and acceleration of the principle motor, but also on the set stiffness of the system. In order to ensure that the position of the foot can be timely and effectively controlled during the swing phase, the optimal range of stiffness settings has to be determined based on the operating conditions of the principal motor. This will ensure that the appropriate foot clearance from the ground can be maintained, and potential falls can be prevented. To this end, ten full cycles of the previously determined sinusoid corresponding to the maximum speed and acceleration of the principal motor have been conducted for each of the ten equidistantly spaced roller positions in the range of $x \in [0,35]$ mm.

The root mean square error (RMSE) between the instructed and achieved output trajectory of the system was observed across all of these tracking tasks in order to determine the overall system's dynamic tracking performance.

1.3) Step response for stiffness control

In order to identify the response capacity of stiffness control, step response experiments were performed. With three different loads (1Nm, 1.67Nm and 2Nm) mounted on the output frame, the secondary motor was set to drive the rollers from the maximum stiffness (x=0mm) position to the minimum (x=35mm), and then back again. Concurrently, the response time needed for the system to change the stiffness across the entire range of variation was recorded.

2) Use case demonstrations

In order to better understand the properties and the behaviour of the system, a set of demonstrations have been conducted across mock application scenarios. For this purpose, we have built a customized test bench (Fig. 4a) consisting of a controllable motor-driven ground plate that moves vertically to simulate the ground interaction with a 3D printed foot attached to the AVSPA.

2.1) In-vitro gait demonstration and analysis

In order to evaluate the performance of the system in as close to a real-world scenario as we can at this stage of development, a simulated control interaction experiments have been conducted.

Reference gait kinematics of a typical level walking (0.8-1.2 m/s) have been extracted from a publicly available dataset [20]. Specifically, data sample "2014001_C3_05.c3d" was considered, which was collected from an injury-free male subject.

The respective right ankle-foot angle (θ) and torque (T) have been derived using the built-in inverse kinematics and inverse dynamics tools in OpenSim [33]. In addition, since the torque of AVSPA can be calculated as the product of the angular deformation $\Delta\theta$ and the equivalent stiffness K (as per Equation 1), we obtained the reference of equivalent stiffness profile from ankle-foot angle and torque of the gait sample to simply demonstrate the function of active stiffness adjustment. The distance variation between the ground and the ankle is also obtained from the data, and used to control the vertical position of the test bench ground plate (Fig. 4a).

Subsequently, three bench tests have been done to verify the performance of the adjusting mechanism when the proposed system works as passive, semi-active and active ankle prostheses.

When initializing the bench tests, the equilibrium angle θ_{eq} of the AVSPA is set as the ankle-foot angle observed at initial heel-strike, and the ground plate of the test bench is positioned at a distance of 1cm below the heel.

In all three modes, the controlled plantarflexion (CP) of the ankle is achieved by moving the ground plate upwards to simulate initial foot-ground contact. After heel strike (HS), the foot is in contact with the ground plate, resulting in an increase in the ankle-foot angle θ during the CP phase as the ground plate ascending. When the foot is flat on the ground, the shank motion is replicated by the principal motor which rotates the ankle joint to induce controlled dorsiflexion (CD) and consequently leads to a decrease in θ in CD phase.

In active mode, during the PP phase, the principal motor increases the equilibrium angle θ_{eq} actively bending the leaf springs (Fig. 4b) in the dorsiflexion direction and increasing the torque leading to the body propulsion. Additionally, the angle change of the shank relative to the ground is added into the motion of principal motor to simulate the ankle-foot angle θ changed by the shank motion, consistent with that of an intact ankle. At the same time, the ground plate moves downwards to simulate the increasing distance between the ankle joint and the ground surface itself. Therefore, the constraint of the plate on

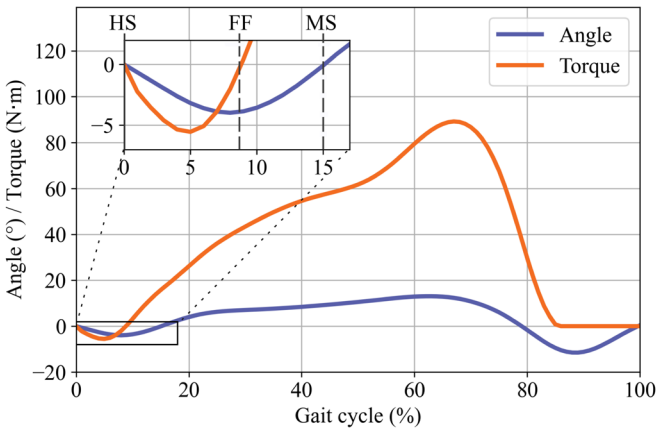

Fig. 7. Ankle-foot angle and torque data during a gait cycle are plotted. Data are from [20]. Data at the beginning of the gait cycle is screened in a subplot. The nadir of the angle curve in the subplot indicates the moment when CP and CP switch occurs, namely, the occurrence of foot-flat (FF) event. At this moment, the torque value has returned to zero earlier than the angle value. The relationship between angle and torque can be linearly approximated before the torque value reaches the nadir; however, this approximation is inapplicable in the latter CP phase when the torque value returns from the nadir to zero.

the foot decreases, leading to an increase in θ. Finally, during the SW phase, because the foot is of the ground, the angular deformation is eliminated. Here, the principal motor controls the equilibrium angle to provide a toe clearance of the ground and simulate the shank motion.

For passive and semi-active modes, since the principal motor does not actively bend the leaf springs to provide additional torque, the principal motor on the prototype only simulates the angle change of the shank relative to the ground, when the ankle joint comes to the end of CD phase. At this point, the ground plate begins to move downwards to imitate the lift-off of the foot. As the distance between the ankle joint and the ground increases, the constraint of the plate on the foot decreases, leading to an increase in θ. After the toe-off (TO) happens,, the prosthesis enters the SW phase. In contrast to the active mode, the equilibrium angle is not additionally supported by the principal motor. Hence, the value of θ will sooner increase to the same value as the equilibrium angle θ_{eq} as the ground plate is descending (Equation 4). Conversely, the motion of the prosthetic ankle enters SW phase earlier than that in the active mode.

In terms of the stiffness adjustment, only the binary switching method is available in the passive mode, while the secondary motor is activated in the semi-active and active modes thus continuously adjusting the stiffness and simulating the nonlinear spring behavior of intact ankle in CD phase. Furthermore, after the artificial foot is off the ground plate, in semi-active and active modes, the stiffness needs to be rapidly increased by the secondary motor to suppress the possible free vibration. This results in stable ankle joint position control, and the stiffness needs to be decreased before the subsequent heel strike thus absorbing the impact.

By analyzing the aforementioned gait data sample it can be observed that the absolute value of ankle torque in the CP phase initially increased and then decreased to 0 Nm when the foot-flat (FF) event happens and just before the start of CD phase (Fig. 7).

However, during the passive and semi-active mode operation, the principal motor is not engaged, as it is used solely to simulate the change in the shank angle. Therefore, the spring loading direction, and with it the torque direction, changes only after the mid-stance (MS) position.

Hence, in the active mode we engage the principal motor close to the end of the CP phase to reset the equilibrium angle while the ankle joint maintains the foot-flat position. This then should correspond closely to the behaviour observed in the real gait data (Fig. 7).

2.2) Human-machine integration demonstration

The proposed prosthetic system provides human-machine interface (HMI) (Fig. 5) in order to enable close volitional interaction with the system. The movement properties of the prosthesis can be estimated and set by analyzing motion relevant signals, such as kinematic and bioelectrical data.

In daily walking, ankle joints often move in periodic gaits with a relatively fixed phase interval on both sides [34]–[36]. Previous studies have proved that, for unilateral amputees, kinematic signals from the intact leg can be used to control the prosthesis on the other leg in real-time, which is called “echo control” [37]–[40].

In this demonstration, the prosthesis is assumed to serve as the bionic ankle on the right side of a user with transtibial amputation. The focus is on the real-time operation of torque/position control and stiffness adjusting, rather than optimal estimator design. Hence, the priority is on kinematics estimation, while the target stiffness is assumed to be in a linear relationship with the ankle-foot angle. A method similar to “echo control” [37]–[40] is adopted to verify the effectiveness of the established human-machine interface. Specifically, the left and right ankle angles were collected synchronously from a healthy male volunteer (29 years old) using MTw Awinda (Xsens Technologies B.V, Netherlands) inertial sensors. Two sensors were places on each leg (one on the top of the foot and one on the shank) and the data was sampled at 80Hz. The data collected from the left ankle was used for estimating to the right ankle properties via an artificial neural network (2 full-connected hidden layers with 128 nodes, ReLU activation function, and 10% dropout rate) with a sliding sample window (length 40 and stride 1) pertaining to the transtibial use case scenario. The measured data of the right ankle served as target labels in the estimator training process.

Since this experiment was conducted under foot suspension condition, the principal motor was used for position control by changing the ankle foot angle through controlling the prosthesis equilibrium angle, which is the same as the methods in the SW phases shown in in-vitro gait demonstrations.

The study was approved by the local ethical board of Aalto University (approval number D/898/03.04/2021). Prior to the experiments, the subject gave their written informed consent in accordance with the Declaration of Helsinki.

IV. Results

A. Stiffness measurement

As illustrated in Fig. 8, the angular deformation and equivalent stiffness exhibit variations as the roller moves. In both directions, the ranges of measured angular deformation are from -29.74° to -0.02° and from 0.01° to 11.17°, while the stiffness ranges from 0.06-87.04 Nm/° and 0.14-169.03 Nm/°, when the roller moves from 0 mm to 35 mm.

From Fig. 8a, it can be observed that on the higher stiffness spring, the RMSE between estimated and measured angular deformation values is 0.5° (or about 4.48% of the entire deformation range of the higher stiffness spring). Likewise, on the lower stiffness spring (within the first 25mm of roller range), the RMSE between estimated and measured angular deformation is 0.4° (or about 1.3% of the entire deformation range of the lower stiffness spring). However, as the roller moves beyond 25mm, the RMSE becomes 4.1° (or about 13.8% of the entire deformation range of the lower stiffness spring).

In Fig. 8b, the stiffness curves plot is divided into two segments to display the data clearly, as the stiffness is relatively large at small angular deformations. The errors between the estimated and measured stiffness reach the peak at the beginning of the roller travel (x=0mm), which are 118.1Nm/° and 241.1Nm/° (or 141.7% and 148.9% of the measured values) on the lower and higher stiffness springs respectively. When the roller moves from 0mm to 14mm, the RMSEs between predicted and measured stiffness were 72.6% and 84.0% of the measured values on the lower and higher stiffness springs. As the rollers traveled in the range of 14 mm to 35mm, the RMSEs decreased to 7.7% and 8.4% of the measured values.

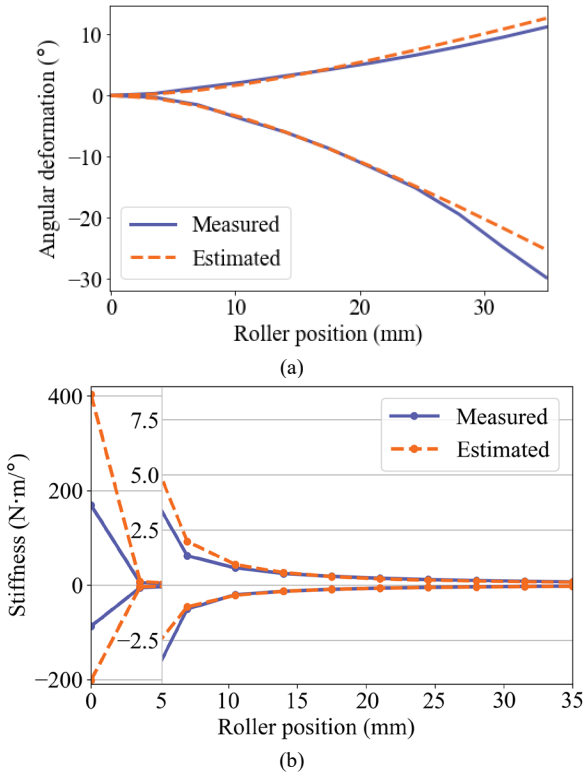

Fig. 8. (a) Angular deformation when roller position varies. The ranges of measured angular deformation are from -29.74° to -0.02° and from 0.01° to 11.17° on the lower and higher stiffness springs. (b) Equivalent stiffness with roller position varies. The plot is divided into two segments, as the stiffness is relatively large at small angular deformations. The RMSEs were 72.6% and 84.0% of the measured values in the range of 0mm to 14mm, and 7.7% and 8.4% in the range of 14mm to 35mm.

B. Sinusoidal tracking for position control

The variation of sinusoidal tracking error with different period lengths and roller positions is shown as Fig. 9. RMSE plots show a decrease with increasing period length and an increase with increasing roller position (decreasing equivalent stiffness).

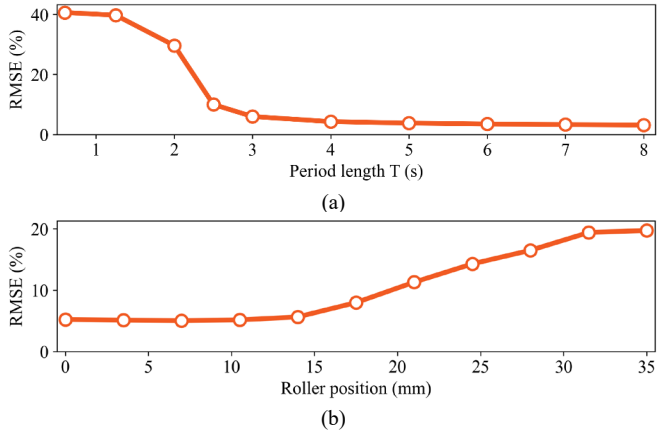

Fig. 9. Sinusoidal tracking errors of position control vary with: (a) cycle lengths (b) roller positions RMSE plots show a decrease with increasing period length and an increase with increasing roller position (decreasing equivalent stiffness).

The RMSE drops to 5.1% of the peak value when the period length T is 3s. Therefore, the available period length T for sinusoidal tracking is decided as T ⩾ 3s, that is, the maximum angular velocity 120°/s and the maximum angular acceleration $14400°/s^2$.

When the period length is 3 seconds, the RMSE increased slightly as the roller moved from 0mm to 14mm. At the roller position of 14mm, the RMSE is 5.6%. Therefore, we set the roller position within 14mm for the SW phases in subsequent use case demonstrations.

C. Step response for stiffness control

As depicted in Fig. 10, the secondary motor takes 0.8s to move the roller from the maximum stiffness position (x=0mm)

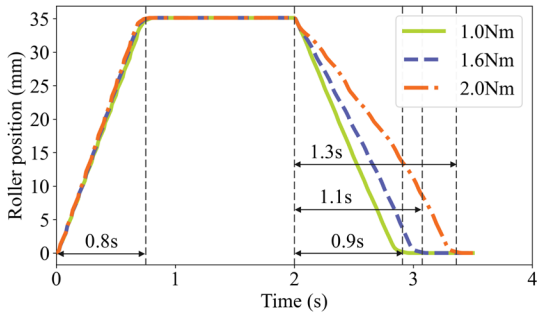

Fig. 10. Step response for position control. The secondary motor takes 0.8 seconds to move the roller from the maximum stiffness position (x=0mm) to the minimum (x=35mm) for all the three loads. While for increasing the stiffness, it takes 0.8s 9s for 1.0Nm load, 1.0s 1s for 1.67 Nm, and 1.3s for 2Nm, respectively.

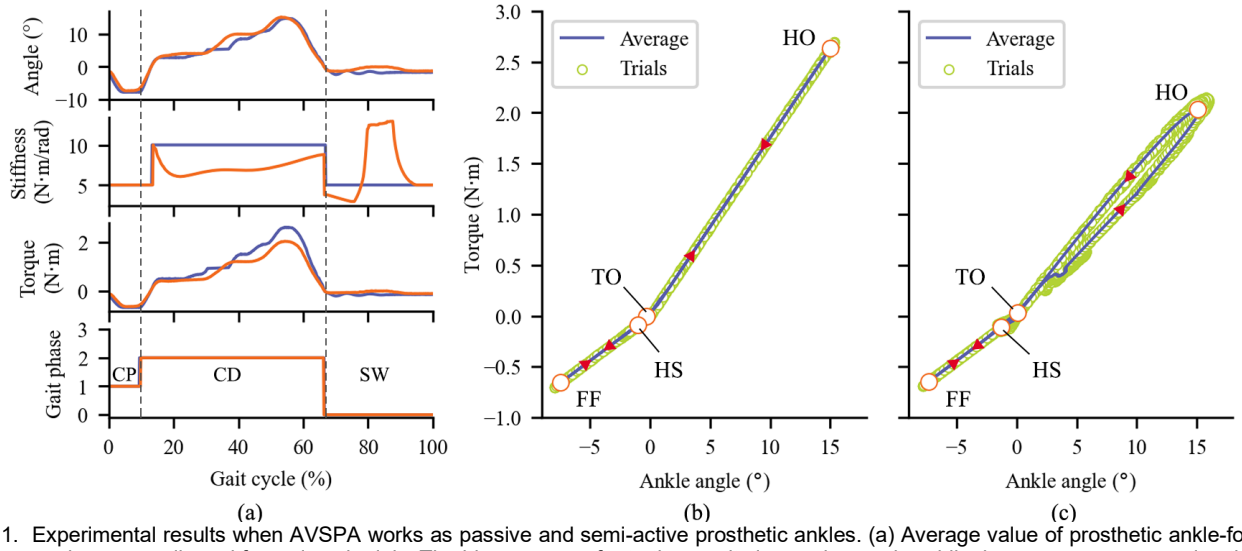

Fig. 11. Experimental results when AVSPA works as passive and semi-active prosthetic ankles. (a) Average value of prosthetic ankle-foot angle, stiffness, and torque, collected from six gait trials. The blue curves refer to the results in passive mode, while the orange curves semi-active mode. (b) Torque versus ankle-foot angle when only binary stiffness switching applied (c)Torque versus ankle-foot angle when both binary stiffness switching and continuous stiffness adjustment applied. Gait events are marked in the plots of torque versus ankle-foot angle, occurring in the order of HS (heel-strike), FF (foot-flat), HO (heel-off), and TO (toe-off). The gait phase CP is between HS and FF, CD between FF and TO, and SW between TO and next HS.

to the minimum (x=35mm) for all the three loads (1Nm, 1.6Nm, 2.0 Nm). While for increasing the stiffness, it takes 0.9s for 1.0Nm load, 1.0s for 1.67 Nm, and 1.3s for 2Nm, respectively. Considering the human walking step frequency [41] and the fact that the change in stiffness happens gradually across this range, this response time can meet the demand of use case demonstration.

D. Use case demonstrations

1) Passive mode: binary stiffness switching

This experiment demonstrates the ability of the proposed AVSPA to switch stiffness with gait phases in a completely passive mode.

Figs. 11a and 11b show the torque-angle characteristic of the system when changing joint stiffness with gait phases only by asymmetric stiffness springs. As can be seen from the stiffness and torque-angle curves, the equivalent stiffness of the prosthesis can be switched when angle is 0° (the mid-stance position), providing compliance even when the secondary motor turned off.

2) Semi-active mode: binary stiffness switching and continuous stiffness adjustment

In the semi-active mode demonstration, the binary stiffness switching and continuous stiffness adjustment are employed.

Fig. 11 shows the gait-cycle data when the stiffness adjusting mechanism actuated. As can be seen in Fig. 11a, the stiffness experiences a rapid jump when the ankle-foot angle goes across the initial equilibrium angle (0°). Fig. 11c shows the torque-angle curve in CD phase is properly adjusted to be two different curves for energy storing and releasing, exhibiting characteristics similar to a nonlinear spring. The stiffness jump makes a quick change without external energy for the secondary motor, which provides the ankle prosthesis with a natural response and compact energy efficiency. Compared with the completely passive mode (Figs. 11a and 11b), the "semi-

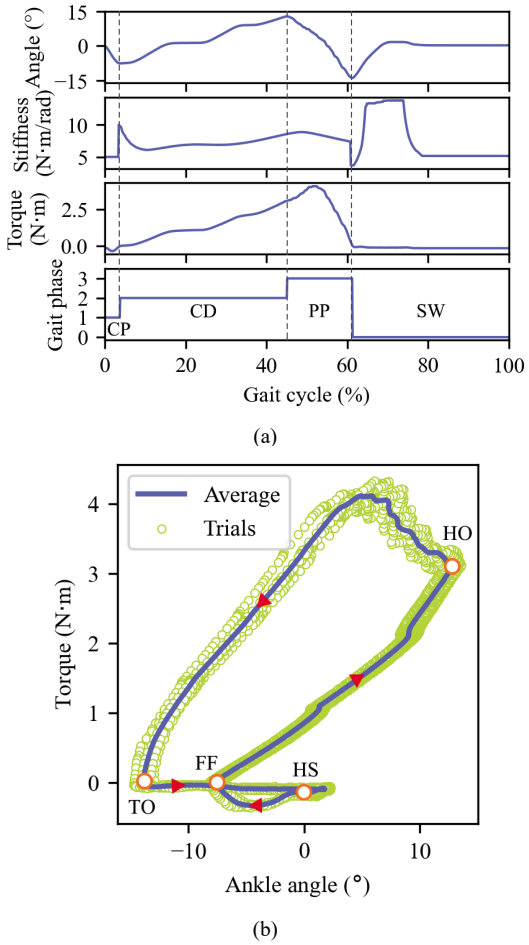

Fig. 12. Experimental results of active mode operation. (a) Average value of prosthetic ankle-foot angle, stiffness, and torque, collected from six gait trials. (b) Torque versus ankle-foot angle when both binary stiffness switching and continuous stiffness adjustment applied. Gait events are marked in the plots of torque versus ankle-foot angle, occurring in the order of HS (heel-strike), FF (foot-flat), HO (heel-off), and TO (toe-off). The gait phase CP is between HS and FF, CD between FF and HO, PP between HO and TO, and SW between TO and next HS.

passive mode" not only prevents excessive impact load during the CP stage, but also can continuously change the stiffness in subsequent phases, to store and release energy in a reasonable way to achieve more compliant behaviors. Moreover, the vibration at the beginning of SW phase shown in the experiment of the passive mode is effectively suppressed when actively increasing the stiffness (see the subplot "Angle" in Fig. 11a).

3) Active mode: Electric propulsion with both binary stiffness switching and continuous stiffness adjustment

In the active mode, the principal motor provides extra torque for body propulsion in the PP phase by actively compressing the leaf spring. Here, the results show that the system can track the desired stiffness during CP and CD, as well as provide extra torque and adjust the stiffness synchronously in PP phase. Specifically, as shown in Fig. 12, the torque was improved by increasing the equilibrium angle in PP phase compared to passive and semi-active modes. Moreover, the joints showed a greater plantar flexion (13.83°) in the later part of the PP phase (see the subplot "Angle" in Fig. 12a) than that in passive mode (2.14°) and semi-passive mode (1.33°). Nonlinear changes of joint stiffness during the CD phase were also observed, as seen in Fig. 12b. Furthermore, the adjustment of equilibrium angle in the later part of the CP phase, allowed the CD phase to start from the foot-flat position and enabled the working spring to be switched earlier than in the passive and semi-active modes, as shown in Figs. 12a and 12b.

E. Human-machine integration demonstration

Fig. 13 shows the experimental data of using the angular position from the left ankle to control the prothesis for the right ankle in two gait cycles.

The first subplot "Left θ" shows the ankle-foot angle change of the subject's left ankle during level-walking, which is used to estimate the ankle-foot angle of the right ankle.

In the subplot "Target right θ", θ_{true} represents the real right ankle-foot angle in coordination with the left ankle, while the ANN-estimated right ankle-foot angle of the prosthesis is shown as θ_{est}. The RMSE between predicted value and true value is 1.8° (or about 6% of the entire ankle-foot angle range).

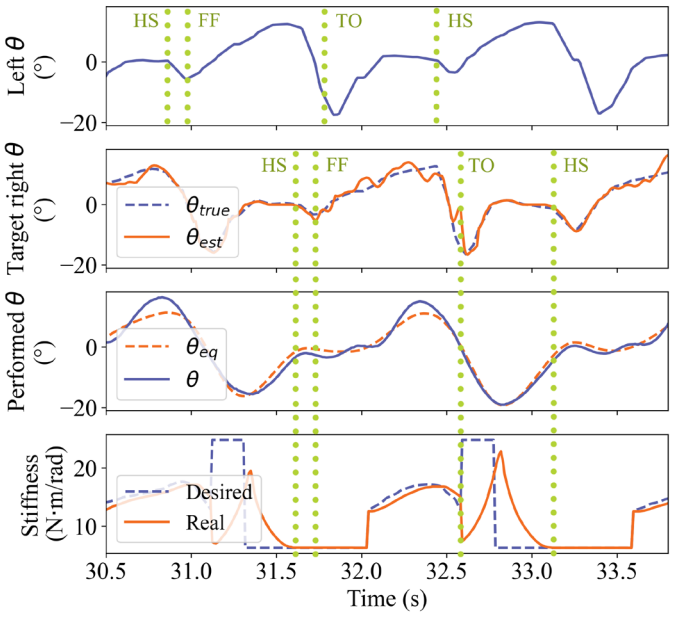

Fig. 13. Kinetic control experiment. Angle flow measured from the left ankle is applied to control the prosthesis which is assumed to be installed on the right lower limb.

With the estimated right ankle-foot angle θ_{est} serves as the target angular position of the principal motor, the performed equilibrium angle θ_{eq} and ankle-foot angle θ of the prosthesis are shown in the subplot "Performed θ". The RMSE between the equilibrium angle θ_{eq} and control command θ_{est} is 8.2° (or about 25.0% of the entire commanded ankle-foot angle range). Due to the unstable vibration, the RMSE of 1.9° (or about 6.1% of the entire the equilibrium angle range) was caused between the ankle foot angle θ and the equilibrium angle θ_{eq}.

In terms of the stiffness adjustment, the RMSE between the real stiffness and desired stiffness in the stance phase (HS to TO) is 0.75Nm/rad (or about 6.9% of the desired stiffness). In the swing phase, after the stiffness was commanded to increase after TO, the real stiffness takes 0.21s to reach the peak (22.87Nm/rad).

V. Discussion

In an effort to efficiently restore the biomechanics and function of intact ankle joints in individual with transtibial amputations, we proposed and evaluated a variable stiffness powered ankle prosthesis (AVSPA) which incorporates a novel asymmetric leaf spring design with bidirectionally distinct inherent stiffness. Previously, similar solutions were either providing bi-directional stiffness switching [11], [21] or continuous stiffness adjustment [27]–[29], [42]–[44]. However, to the best of our knowledge, this is the first solution able to provide both within a single system, which has a potential to enhance the capabilities and converse energy in the users while retaining the compactness of the ankle prosthesis solution.

The proposed AVSPA features leaf springs with intrinsically different stiffnesses in plantar- and dorsi- flexion directions. When coupled with the active stiffness adjustment mechanism, this asymmetric design allows for rapid change in the joint stiffness during CP and CD gait phases (Figs. 11 and 12) which corresponds to the natural ankle control, as observed in biomechanical studies [17], [19], [20]. So, by simply switching the working spring, a rapid increase in stiffness is achieved without external motor participation upon transitioning from CP to CD phase, and the continuous joint stiffness adjustment can continue accordingly.

However, according to the system validation, the mathematical models established to fit the angular deformation and the stiffness (Equations 1 and 3) will produce errors in some intervals of the roller range (Fig. 8). In terms of the angular deformation, this error (RMSE=4.1° or about 13.8% of the entire deformation range of the lower stiffness spring) exists in the roller range of 25mm to 35mm. This deviation can be attributed to the use of a cantilever beam deflection approximation formula in the stiffness model, which exhibits decreased fitting precision when significant deformation occurs. In practical applications, superior results may be yielded through more accurate modelling methods [45]–[47]. In terms

of the stiffness, the fitting error is mostly prominent in the roller range of 0mm to 14mm (RMSE 72.6% and 84.0% of the measured values on the lower and higher stiffness springs). This is because the prototype was fabricated using standard consumer 3D printing with PLA and resin, and manual assembly, resulting in a certain amount of fit clearance between the leaf spring and the roller, which, though small (about 0.5mm), can affect stiffness calculation at small angular deformations via Equation 1. However, as the angular deformation increases, the interference of clearance on stiffness calculation becomes less prominent (RMSE 7.7% and 8.4% on the lower and higher stiffness springs in the roller range of 14mm to 35mm). Nevertheless, the interference caused by the fit clearance does not affect subsequent in-vitro gait demonstrations because the roller moves below 14mm only in the swing (SW) phase, where precise stiffness control is not required. In SW phase, increasing the stiffness is aimed at reducing the free vibration of the foot to provide reliable position control. Whereas, the CP and CD phases are the ones that truly rely on this model for accurate stiffness control. During these phases, the roller displacement ranges from 14mm to 35mm within which RMSE is an order of magnitude lower. Eventually, the effects of fit clearance on stiffness calculation at small deformations can be decreased using more precise manufacturing.

In in-vitro gait demonstrations, the prosthesis avoided excessive impact load through lower stiffness in CP phase. Transition to higher stiffness takes place only when the gait cycle enters into CD phase, which is both in line with natural gait behavior [20] and leads to an improved energy storage. However, when the foot is off the ground (during SW), unstable vibrations may take place due to lower stiffness, which is not desirable and can be unsafe. This issue has been effectively addressed in the semi-active and active mode demonstrations by engaging the secondary motor and increasing the stiffness during the swing (SW) phase (Figs. 11a, 11c and 12).

During the active mode operation, a greater ankle-foot angle (13.83°, see Fig. 12a) is achieved when the foot is off the ground, compared to that in the passive and semi-passive modes (2.14° and 1.33° respectively, see Fig. 11a). This can be attributed to the fact that, upon increasing the equilibrium angle by the principal motor in order to generate propulsive torque, there is a corresponding increase in the ankle-foot angle (during the subsequent foot-off process) releasing the stored energy in the spring (as per Equation 4).

In the human-machine integration demonstration, the ANN adopted is able to predict the right ankle-foot angle (RMSE 1.8° or about 6% of the entire ankle-foot angle range). In the stance phase (HS to TO), the secondary motor was able to track the continuously varying stiffness commands (RMSE 0.75Nm/rad or about 6.9% of the desired stiffness). In the swing phase (TO to next HS), although the motor needed some delay (0.21s) to fully respond to the step command of stiffness, it successfully suppressed the unstable vibrations within the swing phase.

Thanks to the asymmetric design of the spring, compared to powered ankle prostheses that only allow for continuous stiffness adjustment [27]–[29], [42]–[44], the proposed AVSPA can deliver a rapid change in stiffness when transitioning from CP to CD phase (as seen in Fig. 11) with a potential for more compact design and higher energy efficiency. Furthermore, unlike powered ankle prostheses that only permit binary stiffness switching [11], [21], the AVSPA enables continuous stiffness adjustment to better align with the biomechanical characteristics of the intact ankle joint, as shown in Fig. 12. The compatibility between the binary and continuous stiffness adjustment approaches is essentially realized through the spring-roller-spring arrangement in the adjustment mechanism. Additionally, the self-locking property of the lead screw mechanism helps the roller position to be maintained without the need for the secondary motor to remain engaged. This can effectively reduce energy consumption and heat generation of the secondary motor.

Furthermore, the application of leaf springs obviates the need for generating work in the direction of spring deformation by the secondary motor, as reported in prior studies of powered ankle prostheses using VSA [27]–[29]. This design reduces the dependency on a gearbox in order to elevate the torque of the second motor as it is only partially exposed to the load inferred by the user. Together with the asymmetric stiffness, the system has a potential for superior performance in terms of size, energy efficiency, heat dissipation, and adjustment speed.

Wille these initial results seem to be promising, in order to fully evaluate the performance of the system further clinical validation with user compatible version of the AVSPA is needed. This will require development of an optimized control strategy, employment of more robust manufacturing processes, and the construction of a socket interface between AVSPA and amputees. However, the conducted tests were a necessary first step in order to demonstrate the feasibility of the proposed design.

VI. Conclusion

Here, an asymmetric variable stiffness powered ankle prosthesis (AVSPA) with continuous stiffness control and binary stiffness switching is proposed. The core idea is a novel asymmetric VSA inspired by ankle biomechanics between and in specific gait phases. Based on biomechanical data of ankle joint collected from healthy individuals during level walking, we found that in addition to continuous changes in quasi-stiffness, there is also a rapid stiffness change that occurs with changes in joint rotational direction when CD is switched to CP. Therefore, a leaf spring with the bidirectionally asymmetric intrinsic stiffness is integrated into the VSA to realize the similar stiffness modulation. During bidirectional rotation, springs with different stiffness are activated, so stiffness jumps can be achieved without the secondary motor being activated. This design provides a natural stiffness response synchronized with gait changes, as well as reduces motor work, and reduces joint size by reducing the required operation range of spring. In addition, we use a lead screw mechanism to move the rollers to change the effective length of leaf springs so as to continuously adjust the stiffness on the unilateral working spring. Moreover, due to the self-locking characteristics of the lead screw, the stiffness regulating motor can be turned off to save energy

while maintaining the stiffness.

This study advanced the asymmetric stiffness spring in the application of variable stiffness prosthetic ankle, which effectively improves the walking compliance, controllability, and comfort for amputees through enhanced responsiveness to gait phases. This allows for faster adaptation to powered ankle prostheses and effective restoration of motor function. Moreover, it opens up new avenues for the design of compliant powered prostheses. However, further clinical tests are yet to be completed which will drive the final design.

REFERENCES

[1] C. L. McDonald, S. Westcott-McCoy, M. R. Weaver, J. Haagsma, and D. Kartin, "Global prevalence of traumatic non-fatal limb amputation," *Prosthetics Orthot. Int.*, vol. 45, no. 2, pp. 105–114, Apr. 2021, doi: 10.1177/0309364620972258.

[2] R. Al Agha, H. Muneer, and A. Alqaseer, "Major Lower Limb Amputation : Causes, Characteristics and Complications," *Bahrain Med. Bull.*, vol. 39, no. 3, pp. 159–161, Sep. 2017, doi: 10.12816/0047632.

[3] World Health Organization, "Assistive technology," 2018. https://www.who.int/news-room/fact-sheets/detail/assistive-technology (accessed Feb. 26, 2022).

[4] A. F. Azocar, L. M. Mooney, J. F. Duval, A. M. Simon, L. J. Hargrove, and E. J. Rouse, "Design and clinical implementation of an open-source bionic leg," *Nat. Biomed. Eng.*, vol. 4, no. 10, pp. 941–953, 2020, doi: 10.1038/s41551-020-00619-3.

[5] B. Lawson, H. A. Varol, A. Huff, E. Erdemir, and M. Goldfarb, "Control of Stair Ascent and Descent With a Powered Transfemoral Prosthesis," *IEEE Trans. Neural Syst. Rehabil. Eng.*, vol. 21, no. 3, pp. 466–473, May 2013, doi: 10.1109/TNSRE.2012.2225640.

[6] N. Thatte and H. Geyer, "Toward Balance Recovery With Leg Prostheses Using Neuromuscular Model Control," *IEEE Trans. Biomed. Eng.*, vol. 63, no. 5, pp. 904–913, May 2016, doi: 10.1109/TBME.2015.2472533.

[7] M. Cempini, L. J. Hargrove, and T. Lenzi, "Design, development, and bench-top testing of a powered polycentric ankle prosthesis," in *2017 IEEE/RSJ International Conference on Intelligent Robots and Systems (IROS)*, Sep. 2017, pp. 1064–1069. doi: 10.1109/IROS.2017.8202276.

[8] Ottobock, "Instructions for use (user)| 1A1-2 Empower," Salt Lake City.

[9] A. L. Hof, B. A. Geelen, and J. Van den Berg, "Calf muscle moment, work and efficiency in level walking; Role of series elasticity," *J. Biomech.*, vol. 16, no. 7, pp. 523–537, Jan. 1983, doi: 10.1016/0021-9290(83)90067-2.

[10] A. H. Hansen, D. S. Childress, S. C. Miff, S. A. Gard, and K. P. Mesplay, "The human ankle during walking: implications for design of biomimetic ankle prostheses," *J. Biomech.*, vol. 37, no. 10, pp. 1467–1474, Oct. 2004, doi: 10.1016/j.jbiomech.2004.01.017.

[11] S. K. Au, J. Weber, and H. Herr, "Powered Ankle--Foot Prosthesis Improves Walking Metabolic Economy," *IEEE Trans. Robot.*, vol. 25, no. 1, pp. 51–66, Feb. 2009, doi: 10.1109/TRO.2008.2008747.

[12] B. J. Hafner, J. E. Sanders, J. M. Czerniecki, and J. Fergason, "Transtibial energy-storage-and-return prosthetic devices: A review of energy concepts and a proposed nomenclature," *J. Rehabil. Res. Dev.*, vol. 39, no. 1, pp. 1–11, 2002.

[13] B. E. Lawson, J. Mitchell, D. Truex, A. Shultz, E. Ledoux, and M. Goldfarb, "A Robotic Leg Prosthesis: Design, Control, and Implementation," *IEEE Robot. Autom. Mag.*, vol. 21, no. 4, pp. 70–81, Dec. 2014, doi: 10.1109/MRA.2014.2360303.

[14] A. H. Shultz, B. E. Lawson, and M. Goldfarb, "Variable Cadence Walking and Ground Adaptive Standing With a Powered Ankle Prosthesis," *IEEE Trans. Neural Syst. Rehabil. Eng.*, vol. 24, no. 4, pp. 495–505, Apr. 2016, doi: 10.1109/TNSRE.2015.2428196.

[15] K. W. Hollander, R. Ilg, T. G. Sugar, and D. Herring, "An Efficient Robotic Tendon for Gait Assistance," *J. Biomech. Eng.*, vol. 128, no. 5, pp. 788–791, Oct. 2006, doi: 10.1115/1.2264391.

[16] J. K. Hitt, T. G. Sugar, M. Holgate, and R. Bellman, "An Active Foot-Ankle Prosthesis With Biomechanical Energy Regeneration," *J. Med. Device.*, vol. 4, no. 1, pp. 1–9, Mar. 2010, doi: 10.1115/1.4001139.

[17] S. K. Au, P. Dilworth, and H. Herr, "An ankle-foot emulation system for the study of human walking biomechanics," in *Proceedings 2006 IEEE International Conference on Robotics and Automation, 2006. ICRA 2006.*, pp. 2939–2945. doi: 10.1109/ROBOT.2006.1642148.

[18] D. P. Ferris, M. Louie, and C. T. Farley, "Running in the real world: adjusting leg stiffness for different surfaces," *Proc. R. Soc. London. Ser. B Biol. Sci.*, vol. 265, no. 1400, pp. 989–994, Jun. 1998, doi: 10.1098/rspb.1998.0388.

[19] M. L. Palmer, "Sagittal plane characterization of normal human ankle function across a range of walking gait speeds," Massachusetts Institute of Technology, 2002.

[20] C. Schreiber and F. Moissenet, "A multimodal dataset of human gait at different walking speeds established on injury-free adult participants," *Sci. Data*, vol. 6, no. 1, p. 111, Dec. 2019, doi: 10.1038/s41597-019-0124-4.

[21] S. K. Au, J. Weber, and H. Herr, "Biomechanical Design of a Powered Ankle-Foot Prosthesis," in *2007 IEEE 10th International Conference on Rehabilitation Robotics*, Jun. 2007, pp. 298–303. doi: 10.1109/ICORR.2007.4428441.

[22] L. Jin and M. E. Hahn, "Modulation of lower extremity joint stiffness, work and power at different walking and running speeds.," *Hum. Mov. Sci.*, vol. 58, pp. 1–9, Apr. 2018, doi: 10.1016/j.humov.2018.01.004.

[23] G. Morey-Klapsing, A. Arampatzis, and G.-P. Brüggemann, "Evidence of Proactive Forefoot Control During Landings on Inclined Surfaces," *J. Mot. Behav.*, vol. 39, no. 2, pp. 89–102, Mar. 2007, doi: 10.3200/JMBR.39.2.89-102.

[24] A. S. Voloshina and D. P. Ferris, "Biomechanics and energetics of running on uneven terrain," *J. Exp. Biol.*, vol. 218, no. 5, pp. 711–719, Mar. 2015, doi: 10.1242/jeb.106518.

[25] C. T. Farley, H. H. P. Houdijk, C. Van Strien, and M. Louie, "Mechanism of leg stiffness adjustment for hopping on surfaces of different stiffnesses," *J. Appl. Physiol.*, vol. 85, no. 3, pp. 1044–1055, Sep. 1998, doi: 10.1152/jappl.1998.85.3.1044.

[26] J. Sinclair, S. Atkins, and P. J. Taylor, "The Effects of Barefoot and Shod Running on Limb and Joint Stiffness Characteristics in Recreational Runners," *J. Mot. Behav.*, vol. 48, no. 1, pp. 79–85, Jan. 2016, doi: 10.1080/00222895.2015.1044493.

[27] L. Flynn, J. Geeroms, R. Jimenez-Fabian, B. Vanderborght, N. Vitiello, and D. Lefeber, "Ankle-knee prosthesis with active ankle and energy transfer: Development of the CYBERLEGs Alpha-Prosthesis," *Rob. Auton. Syst.*, vol. 73, pp. 4–15, Nov. 2015, doi: 10.1016/j.robot.2014.12.013.

[28] R. Van Ham, B. Vanderborght, M. Van Damme, B. Verrelst, and D. Lefeber, "MACCEPA, the mechanically adjustable compliance and controllable equilibrium position actuator: Design and implementation in a biped robot," *Rob. Auton. Syst.*, vol. 55, no. 10, pp. 761–768, Oct. 2007, doi: 10.1016/j.robot.2007.03.001.

[29] R. Jimenez-Fabian, L. Flynn, J. Geeroms, N. Vitiello, B. Vanderborght, and D. Lefeber, "Sliding-Bar MACCEPA for a Powered Ankle Prosthesis," *J. Mech. Robot.*, vol. 7, no. 4, Nov. 2015, doi: 10.1115/1.4029439.

[30] T. Morita and S. Sugano, "Design and development of a new robot joint using a mechanical impedance adjuster," in *Proceedings of 1995 IEEE International Conference on Robotics and Automation*, vol. 3, pp. 2469–2475. doi: 10.1109/ROBOT.1995.525630.

[31] J. Choi, S. Hong, W. Lee, S. Kang, and M. Kim, "A Robot Joint With Variable Stiffness Using Leaf Springs," *IEEE Trans. Robot.*, vol. 27, no. 2, pp. 229–238, Apr. 2011, doi: 10.1109/TRO.2010.2100450.

[32] M. K. Shepherd and E. J. Rouse, "The VSPA foot: A quasi-passive ankle-foot prosthesis with continuously variable stiffness," *IEEE Trans. Neural Syst. Rehabil. Eng.*, vol. 25, no. 12, pp. 2375–2386, 2017, doi: 10.1109/TNSRE.2017.2750113.

[33] S. L. Delp *et al.*, "OpenSim: Open-Source Software to Create and Analyze Dynamic Simulations of Movement," *IEEE Trans. Biomed. Eng.*, vol. 54, no. 11, pp. 1940–1950, Nov. 2007, doi: 10.1109/TBME.2007.901024.

[34] R. E. Hannah, J. B. Morrison, and A. E. Chapman, "Kinematic symmetry of the lower limbs.," *Arch. Phys. Med. Rehabil.*, vol. 65, no. 4, pp. 155–8, Apr. 1984.

[35] J. Hamill, B. T. Bates, and K. M. Knutzen, "Ground Reaction Force Symmetry during Walking and Running," *Res. Q. Exerc. Sport*, vol. 55, no. 3, pp. 289–293, Sep. 1984, doi: 10.1080/02701367.1984.10609367.

[36] L. A. Gundersen, D. R. Valle, A. E. Barr, J. V Danoff, S. J. Stanhope, and L. Snyder-Mackler, "Bilateral Analysis of the Knee and Ankle

During Gait: An Examination of the Relationship Between Lateral Dominance and Symmetry," *Phys. Ther.*, vol. 69, no. 8, pp. 640–650, Aug. 1989, doi: 10.1093/ptj/69.8.640.

[37] W. C. Flowers and R. W. Mann, "An electrohydraulic knee-torque controller for a prosthesis simulator.," *J. Biomech. Eng.*, vol. 99, no. 1, pp. 3–8, Feb. 1977, doi: 10.1115/1.3426266.

[38] D. L. Grimes, "An active multi-mode above knee prosthesis controller," Massachusetts Institute of Technology, 1979.

[39] J. L. Stein, "Design issues in the stance phase control of above-knee prostheses," Massachusetts Institute of Technology, 1983.

[40] Össur, "POWER KNEE PKA01 Instructions for use," Reykjavík, 2022.

[41] A. Tanaka *et al.*, "Age-Related Changes in Natural and Fast Walking," *Percept. Mot. Skills*, vol. 80, no. 1, pp. 217–218, Feb. 1995, doi: 10.2466/pms.1995.80.1.217.

[42] B. J. Bergelin, J. O. Mattos, J. G. Wells, and P. A. Voglewede, "Concept Through Preliminary Bench Testing of a Powered Lower Limb Prosthetic Device," *J. Mech. Robot.*, vol. 2, no. 4, Nov. 2010, doi: 10.1115/1.4002205.

[43] B. J. Bergelin and P. A. Voglewede, "Design of an Active Ankle-Foot Prosthesis Utilizing a Four-Bar Mechanism," *J. Mech. Des.*, vol. 134, no. 6, Jun. 2012, doi: 10.1115/1.4006436.

[44] D. Dong, W. Ge, B. Convens, Y. Sun, T. Verstraten, and B. Vanderborght, "Design, Optimization and Energetic Evaluation of an Efficient Fully Powered Ankle-Foot Prosthesis With a Series Elastic Actuator," *IEEE Access*, vol. 8, pp. 61491–61503, 2020, doi: 10.1109/ACCESS.2020.2983518.

[45] Y.-Q. Yu, S.-K. Zhu, Q.-P. Xu, and P. Zhou, "A novel model of large deflection beams with combined end loads in compliant mechanisms," *Precis. Eng.*, vol. 43, pp. 395–405, Jan. 2016, doi: 10.1016/j.precisioneng.2015.09.003.

[46] A. Kimiaeifar, N. Tolou, A. Barari, and J. L. Herder, "Large deflection analysis of cantilever beam under end point and distributed loads," *J. Chinese Inst. Eng.*, vol. 37, no. 4, pp. 438–445, May 2014, doi: 10.1080/02533839.2013.814991.

[47] J. Zhang and G. Liu, "Simple Computational Methods for Large Deformation of Plate-Spring End Imposed by Varying Load," in *2015 14th International Symposium on Distributed Computing and Applications for Business Engineering and Science (DCABES)*, Aug. 2015, pp. 402–406. doi: 10.1109/DCABES.2015.107.